Díaz-Rubio, Ana; Li, Junfei; Shen, Chen; Cummer, Steven A.; Tretyakov, Sergei A.

Power flow–conformal metamirrors for engineering wave reflections

Published in:
Science Advances

DOI:
10.1126/sciadv.aau7288

Published: 15/02/2019

Document Version
Publisher's PDF, also known as Version of record

APPLIED PHYSICS

Power flow–conformal metamirrors for engineering wave reflections

Ana Díaz-Rubio[1]*, Junfei Li[2], Chen Shen[2], Steven A. Cummer[2], Sergei A. Tretyakov[1]

Recently, the complexity behind manipulations of reflected fields by metasurfaces has been addressed, showing that, even in the simplest scenarios, nonlocal response and excitation of auxiliary evanescent fields are required for perfect field control. In this work, we introduce purely local reflective metasurfaces for arbitrary manipulations of the power distribution of reflected waves without excitation of any auxiliary evanescent field. The method is based on the analysis of the power flow distribution and the adaptation of the reflector shape to the desired distribution of incident and reflected fields. As a result, we find that these power-conformal metamirrors can be easily implemented with conventional passive unit cells. The results can be used for the design of reflecting surfaces with multiple functionalities and for waves of different physical nature. In this work, we present the cases of anomalous reflection and beam splitting for both acoustic and electromagnetic waves.

INTRODUCTION

Metasurfaces, the two-dimensional (2D) versions of metamaterials, have opened new possibilities to control scattering of waves, with many applications in thin-sheet polarizers, beam splitters, beam steerers, lenses, and more (*1*–*3*). The interest in thin structures capable of controlling and transforming impinging waves increased after the formulation of the generalized reflection and refraction law (GSL) (*4*), which states that, by using small phase-shifting elements, it is possible to control the directions of reflected and transmitted waves. Among all possible scenarios where metasurfaces can be applied, this work is focused on the analysis of reflective metasurfaces, so-called metamirrors.

In this context, the simplest nontrivial functionality is probably the anomalous reflection, which is the phenomenon of plane-wave reflection in directions different from the specular one. Anomalous reflection can be obtained by using conventional diffraction gratings (blazed gratings), where the energy scattered into each propagating Floquet harmonic is carefully engineered (*5*–*7*). The efficiency of these systems, defined as the percentage of the incident power that is sent into the desired direction, can be high only if there is not more than one or two unwanted propagating Floquet modes or in the retroreflection case. Recent studies of the physics of conventional gratings resulted in new possibilities of controlling reflected waves (*8*, *9*). In these systems, by designing the period of the grating, the scattering properties of the constituent inclusions, and the mutual coupling between them, one can engineer the amount of power reflected into different directions. This novel concept, the metagratings, has shown promising results for both anomalous reflection and beam splitting (both systems allow propagation of only three Floquet harmonics). It is important to mention that the unit cells of the inclusions are not necessarily small in comparison with the wavelength and, for these examples, only one element per period gives enough degrees of freedom for controlling the energy distributed into the three harmonics allowed in the system. As the number of propagating harmonics increases, more inclusions have to be considered, and the analytical solutions become too involved, as they must account for interactions of many different inclusions in the unit cell. For this reason, it is difficult to extend this method to more general and complex distributions of fields, where the amplitude, phase, and direction of numerous reflected waves should be fully controlled, or to nonperiodic systems, such as lenses.

Metasurfaces, which allow subwavelength-scale control of fields, have been proposed as an alternative to gratings, potentially offering full control over the reflection directions, when the number of potentially propagating Floquet modes can be arbitrarily large. In the design of metasurfaces, local response of the constitutive elements is commonly assumed. This assumption has two important implications. First, for a given application, the metasurface can be homogenized and the required properties of the constituent elements can be easily found. Second, the constituent meta-atoms can be individually designed. Despite the simplicity of the anomalous reflection problem, which has been extensively studied for electromagnetic (*4*, *10*, *11*) and acoustic (*12*–*15*) waves, it was only recently that the physics of this wave transformation by metasurfaces was properly understood (*16*–*23*). In particular, it was shown that phase-gradient metasurfaces designed on the basis of the generalized reflection law (*4*) can have high efficiencies only if the deflection angle does not exceed 40° to 45° (*18*, *21*).

To understand the difficulties related to control of reflections from metasurfaces, one can consider power flow in the vicinity of anomalous reflectors. Here, multiple propagating waves with different transverse wave numbers coexist in one medium, and the interference between them results in inhomogeneous power flow profiles, where the power flow vector crosses the metasurface plane. In other words, there will be regions where the power carried by the desired distribution of the incident and reflected waves "enters" the metasurface and other regions where the power "emerges" from the surface. It means that the metasurface requires periodically distributed gain/loss response (*17*) or strongly nonlocal behavior (*9*, *16*, *18*, *20*).

It was shown theoretically that the nonlocal properties, required for high-efficiency reflections into arbitrary directions, can be, in principle, realized by carefully engineering the surface reactance profile (*20*). The first known experimental realizations of perfect anomalous reflectors were based on numerical optimizations (*18*, *21*), because the intrinsically nonlocal behavior of any meta-atom combined with the goal to engineer the nonlocal properties of many interacting meta-atoms complicates the implementation of all nonlocal solutions. The next step toward full engineering of wave reflection is the simultaneous control of two reflected waves. As it was demonstrated in (*24*), flat beam splitting

[1]Department of Electronics and Nanoengineering, Aalto University, P.O. Box 15500, FI-00076 Aalto, Finland. [2]Department of Electrical and Computer Engineering, Duke University, Durham, NC 27708, USA.
*Corresponding author. Email: ana.diazrubio@aalto.fi

metasurfaces also require strong nonlocal responses and, consequently, the use of numerical optimizations. Finding possibilities for controlling multiple reflected waves without parasitic reflections using local metasurfaces can open new avenues for the design of highly efficient devices such as holograms or lenses. To recover the local response of the metasurface, Epstein and Eleftheriades proposed the use of auxiliary evanescent fields behind the metasurface as a power-guiding mechanism (*19*). In this scenario, the required nonlocal interactions between meta-atoms are realized using carefully engineered evanescent fields behind the surface. This solution requires full control of the bianisotropic response of the meta-atoms that can complicate the implementation, especially at high frequencies. In addition, the complexity of the evanescent fields that ensure the nonlocal coupling of meta-atoms will increase for more sophisticated applications.

Here, we study the possibility of creating metamirrors that are capable of reflecting waves into arbitrary directions without parasitic scattering and without the need for any evanescent fields close to the metasurface. In this scenario, the fields in front of the metamirror are perfect combinations of the desired propagating plane waves in the far zone and in the vicinity of the metasurface. Absence of evanescent fields in front of the metamirror implies that the response is local and that it is possible to design metamirrors using analytical formulas, without any further numerical optimization of complex nonlocal structures. We approach the problem by analyzing the distributions of propagating power flow in the desired set of plane waves, not restricting the study to waves of a specific physical nature. Previously, analysis of the power flow distribution has been used for studying surface-relief gratings (*6*), where the metallic (or dielectric) shape of the grating can be designed to control the energy scattered into a specific diffraction mode. However, these solutions do not ensure exact fulfillment of the boundary conditions on the surface. The method proposed here allows us to design theoretically perfect anomalous reflectors with rather general functionalities. Illustrations are provided for anomalous reflectors and beam splitters. The derivations are made for acoustic and electromagnetic (see the Supplementary Materials) scenarios.

RESULTS

Design methodology

In this section, we provide a systematic methodology for the design of theoretically perfect metamirrors. The approach comprises four steps: (i) definition of the fields for the desired functionality, satisfying the global power balance (all the incident energy is reflected by the metasurface); (ii) analysis of the power flow distribution and definition of the conformal surface; (iii) surface impedance calculation; and (iv) implementation with passive elements.

Anomalous reflective metamirror

We begin by considering the anomalous reflection scenario where, requiring the absence of any parasitic reflections, we define an incident sound plane wave and a reflected plane wave with the directions of propagation θ_i and θ_r, respectively. Figure 1A shows a schematic representation of the problem when $\theta_i = 0°$. Pressure field in this scenario can be expressed as

$$p(r) = p_0\left[e^{-j\mathbf{k}_i\cdot\mathbf{r}} + Re^{-j\mathbf{k}_r\cdot\mathbf{r}}\right] \quad (1)$$

where $\mathbf{k}_i = k(\sin\theta_i\hat{\mathbf{x}} - \cos\theta_i\hat{\mathbf{y}})$, $\mathbf{k}_r = k(\sin\theta_r\hat{\mathbf{x}} + \cos\theta_r\hat{\mathbf{y}})$, $k = \omega/c$ is the wave number in the medium, p_0 is the amplitude of the incident plane wave, and $R = |R|e^{j\phi_r}$ is the reflection coefficient. The components of the velocity vector $\mathbf{v}(r) = v_x(r)\hat{\mathbf{x}} + v_y(r)\hat{\mathbf{y}}$ associated with this pressure field read

$$v_x(r) = \frac{p_0}{\eta_0}\left[\sin\theta_i e^{-j\mathbf{k}_i\cdot\mathbf{r}} + R\sin\theta_r e^{-j\mathbf{k}_r\cdot\mathbf{r}}\right] \quad (2)$$

$$v_y(r) = \frac{p_0}{\eta_0}\left[-\cos\theta_i e^{-j\mathbf{k}_i\cdot\mathbf{r}} + R\cos\theta_r e^{-j\mathbf{k}_r\cdot\mathbf{r}}\right] \quad (3)$$

with $\eta_0 = \rho c$ being the characteristic impedance of the medium. As it was demonstrated in (*16*, *17*, *20*), to ensure perfect conversion between the incident and the reflected plane waves, avoiding scattering of energy into any other direction, the amplitude of the reflection coefficient has to satisfy $|R| = \sqrt{\cos\theta_i/\cos\theta_r}$.

For proper understanding of the problem, we need to examine the intensity vector distribution. The x and y components of the intensity vector can be written as

$$I_x = I_0[A + |R|(\sin\theta_i + \sin\theta_r)\cos(\Delta\mathbf{k}\cdot\mathbf{r} + \phi_r)] \quad (4)$$

$$I_y = I_0|R|(\cos\theta_r - \cos\theta_i)\cos(\Delta\mathbf{k}\cdot\mathbf{r} + \phi_r) \quad (5)$$

where $A = \sin\theta_i + |R|^2\sin\theta_r$, $\Delta\mathbf{k} = k[(\sin\theta_i - \sin\theta_r)\hat{\mathbf{x}} - (\cos\theta_i + \cos\theta_r)\hat{\mathbf{y}}]$, and $I_0 = \frac{1}{2}\frac{p_0^2}{\eta_0}$. The first term in Eq. 4 can be interpreted as the contributions of the incident and reflected plane waves. The second term describes the spatial modulations of the power flow due to the interference of these two waves. Equation 5 shows that there is a periodically varying power flow in the normal direction due to the interference of the incident and reflected waves. The physical meaning and consequences of the power modulation have been studied in (*16*–*23*).

Figure 1B shows the distribution of the intensity vector when $\phi_r = 0$, $\theta_i = 0°$, and $\theta_r = 70°$. Detailed inspection reveals that for any horizontal line, for example, $y = 0$, where one can position a flat metamirror, the intensity vector crosses the surface. This behavior can be described in terms of a complex surface impedance (*16*, *20*), where the real part takes positive and negative values, corresponding to "loss" or "gain" inside the metamirror. It is worth noting that the value of the reflection coefficient has been chosen to ensure the overall power balance between the incident and reflected energies. Thus, loss and gain compensate each other when averaged over the metasurface period. If the surface is passive and lossless, the periodic modulation of the energy crossing the boundary can be possibly realized, arranging some channeling of energy along the metasurface plane, which requires strongly nonlocal (spatially dispersive) properties.

Locally responding lossless metasurfaces can be realized only if the real part of the surface impedance is zero, which means that the power is allowed to flow only along the surface without crossing the metasurface boundary. This condition can be satisfied by defining a specific spatial profile of the metasurface, which would be at all points tangential to the power flow of the desired set of the incident and reflected fields. In this case, energy neither enters nor emerges from the metasurface. To find these spatial profiles, we introduce a vector field, which is everywhere tangential to the power flow. First, we define a vector perpendicular to the intensity vector as $\mathbf{N} = -I_y\hat{\mathbf{x}} + I_x\hat{\mathbf{y}}$. Then, we define a scalar function

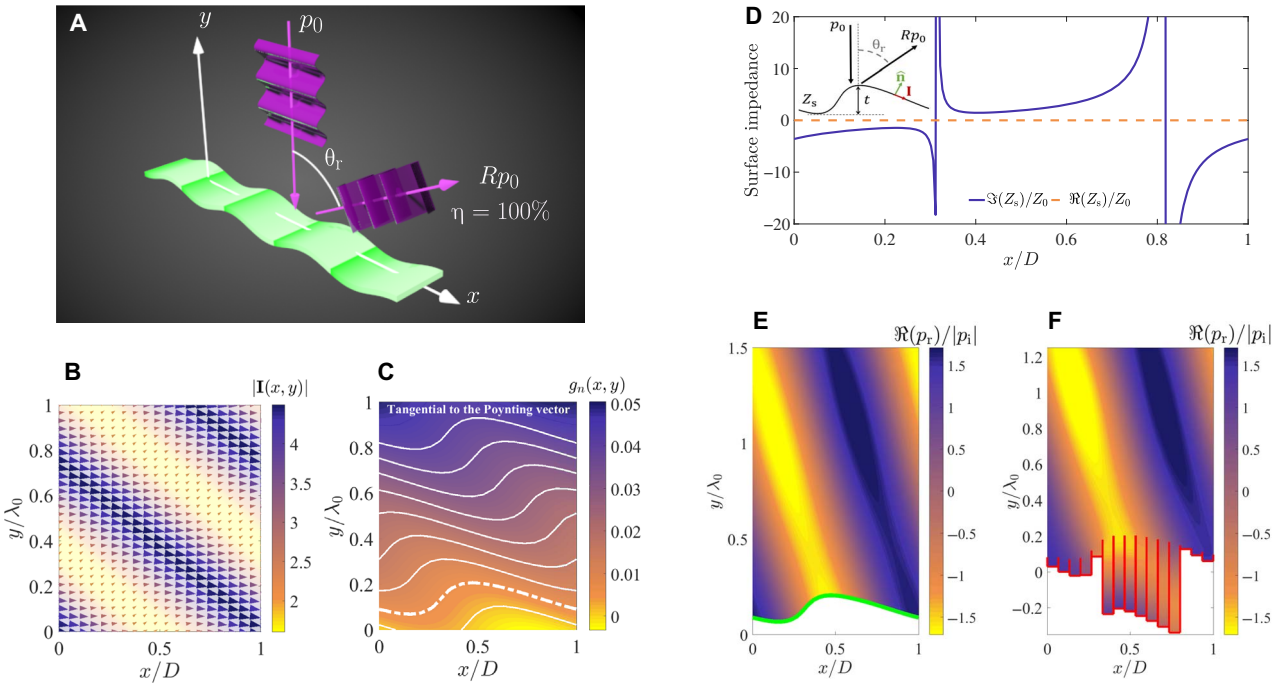

Fig. 1. Anomalous reflective metamirror. The study is carried out for $\phi_r = 0$, $\theta_i = 0°$, and $\theta_r = 70°$. (**A**) Schematic representation of the problem. (**B**) Distribution of the intensity vector dictated by Eqs. 4 and 5. The period of the metasurface can be calculated as $D = \lambda_0/|\sin\theta_i - \sin\theta_r|$, where λ_0 is the wavelength at the operation frequency. (**C**) The normalized curve level function $g_n(x, y) = g(x, y)/I_0$. White lines represent the level curves, i.e., the curves parallel to the intensity vector at every point. (**D**) Surface impedance. The corresponding level curve associated with this impedance is marked with the dashed line in (C). Numerical simulation of the response of a power-conformal metasurface: (**E**) Metasurface modeled as an inhomogeneous reactive boundary. The green line shows the boundary surface. (**F**) Actual implementation using rigidly ended tubes. Red lines indicate surfaces modeled as hard boundaries.

$g(x, y)$ such that $\nabla g(x, y) = \mathbf{N}$. Note that, because of the properties of the gradient, the level curves of the function $g(x, y)$ are tangential to the intensity vector. Hence, the function $g(x, y)$ represents the power potential so that the energy does not flow along its level curves. In the particular case of anomalous reflection, $g(x, y)$ reads

$$g(x, y) = I_0[Ay + B\sin(\Delta\mathbf{k}\cdot\mathbf{r}) + C] \quad (6)$$

where $B = \frac{|R|}{k}\frac{\cos\theta_i - \cos\theta_r}{\sin\theta_i - \sin\theta_r}$ and C is a constant. By analyzing the spatial distribution of the function $g(x, y)$, we identify the level curves of the function $g(x, y)$, which can be described as $y = f(x)$. Figure 1C represents the function $g(x, y)$ and the curves at which it is constant for our example of $\phi_r = 0$, $\theta_i = 0°$, and $\theta_r = 70°$. At any curve given by Eq. 6, the power flow is tangential to this curve. Thus, at these curves, we can terminate the field domain by a boundary modeled by a purely imaginary, reactive input impedance.

To realize a perfectly reflecting metamirror, we select one of these curves and calculate the corresponding impedance. To do that, we define the normalized normal vector to such power-conformal metasurface as $\hat{\mathbf{n}} = \mathbf{N}/|\mathbf{N}|$ (see the inset in Fig. 1D). In terms of this vector, the surface impedance is defined as

$$Z_s(x) = \frac{p(x, y_c)}{-\hat{\mathbf{n}}\cdot\mathbf{v}(x, y_c)} \quad (7)$$

This impedance is represented in Fig. 1D, where we can see that the real part is identically zero, meaning that a local and lossless design is possible. We have numerically corroborated this finding using a numerical simulation, where the metasurface is modeled as a boundary impedance (*25*). The results are shown in Fig. 1E, where the scattered pressure is plotted. The green line shows the position of the impedance boundary that models the metasurface. The efficiency of the design is 99%. It is important to mention that the maximum amplitude (defined as the distance between the maximum and minimum position) of the contour modulation, t, is small in terms of the wavelength $t = \lambda/7$.

Owing to the local, passive, and lossless nature of the impedance shown in Fig. 1D, we can easily design and realize a curved metamirror providing the desired response. As a proof of concept, we use the simplest phase shifters, rigidly ended tubes. The input impedance of each tube can be found as $Z_{s,i} = -j\eta_0\cot(kl_i)$, where l_i is the length of each tube (*26*). It is important to mention that such treatment as a purely imaginary impedance is justified if the tubes are thick enough so that losses can be neglected. In practice, this condition limits the maximum number of elements per period. We select the length of each tube according to Eq. 7, and this completes the design. For the particular example of an anomalous reflector for $\theta_i = 0°$ and $\theta_r = 70°$, Fig. 1F shows the scattered pressure of the final design implemented with terminated tubes. Red lines show the tube walls modeled as hard boundary conditions. Specifically, in each period, we use 15 tubes with the following lengths: $0.0524\lambda_0$, $0.0699\lambda_0$, $0.0874\lambda_0$, $0.0961\lambda_0$, $0.0349\lambda_0$, $0.4156\lambda_0$, $0.4068\lambda_0$, $0.4243\lambda_0$, $0.4418\lambda_0$, $0.4563\lambda_0$, $0.4738\lambda_0$, $0.4884\lambda_0$, $0.0029\lambda_0$, $0.0204\lambda_0$, and $0.0349\lambda_0$. The efficiency of the anomalous reflector is $\eta^{sim}_{periodic} = 99\%$, without any numerical optimization. Notice that viscous and thermal losses are not considered in this calculation (more information about the losses is given in the analysis of the experimental results).

Such a simple design based on analytical expressions becomes possible because power-conformal metamirrors do not need excitation and careful engineering of reactive, evanescent fields in the vicinity of the metasurface. Each small portion of the surface responds locally to the fields at its location. It is important to mention that, to reduce the overall thickness of the device, any other phase shifter, such as labyrinthine cells (*12*, *15*), can potentially be used without affecting the performance. The same approach can be used as a systematic design method for anomalous reflectors for any desired incidence and reflection directions, or even more complicated fields.

Beam splitting metamirror

The introduced method can be used for the creation of more complex field distributions and for other functionalities. Here, we provide an example of a metasurface capable of splitting waves coming from a certain direction into two reflected waves, propagating along two different desired directions. As it was shown in (*24*), this functionality also requires nonlocal response or additional evanescent fields. In this case, the pressure field can be expressed as

$$p(r) = p_0\left[e^{-j\mathbf{k}_i\cdot\mathbf{r}} + R_1 e^{-j\mathbf{k}_{r1}\cdot\mathbf{r}} + R_2 e^{-j\mathbf{k}_{r2}\cdot\mathbf{r}}\right] \quad (8)$$

where $R_1 = |R_1|e^{j\phi_1}$ and $R_2 = |R_2|e^{j\phi_2}$ represent the relative complex amplitudes of the reflected waves. As an example, we assume that the metasurface is illuminated normally, $\theta_i = 0°$, and the reflected beams are sent into $\pm\theta_r$ (see Fig. 2A). In this case, the corresponding wave numbers read $\mathbf{k}_i = k\hat{\mathbf{y}}$, $\mathbf{k}_{r1} = k(\sin\theta_r\hat{\mathbf{x}} + \cos\theta_r\hat{\mathbf{y}})$, and $\mathbf{k}_{r2} = k(-\sin\theta_r\hat{\mathbf{x}} + \cos\theta_r\hat{\mathbf{y}})$. This notation allows us to not only model and design symmetric splitters where the incident power is equally divided between the two reflected waves but also realize any other distribution of power between the two waves that fulfills the power conservation condition $(|R_1|^2 + |R_2|^2)\cos\theta_r = 1$. As it has been shown in (*16*), flat metasurfaces for implementing this functionality also require strong nonlocal response. Our aim here is to find a local, passive, and lossless realization by using a power flow–conformal metamirror. Following the same approach as above, we need to find a surface profile $y = f(x)$, where the corresponding surface impedance Z_s is purely imaginary.

First, we find a suitable surface that is tangential to the power flow in the desired set of three plane waves. In this case, the intensity distribution $\mathbf{I}(x,y) = \frac{1}{2}[Re(pv_x^*)\hat{\mathbf{x}} + Re(pv_y^*)\hat{\mathbf{y}}]$ depends on the reflection angle θ_r and on the amplitudes of the reflected waves R_1 and R_2. As an example, we design a metamirror that sends 70 and 30% of the incident power into ±70° and $\phi_1 = \phi_2 = 0$. The corresponding amplitudes of the reflection coefficients are $|R_1| = 1.43$ and $|R_2| = 0.94$. The power flow distribution for this case is shown in Fig. 2B, where we see the intensity modulations produced by interfering incident and reflected waves. The function whose level curves will define the tangential contours to the intensity vector can be expressed as

$$g(x,y) = I_0 G(x) + I_0 F(y) + I_0\frac{\cos\theta_r - 1}{k\sin\theta_r}[R_1\sin(\Delta\mathbf{k}^-\cdot\mathbf{r}) - R_2\sin(\Delta\mathbf{k}^+\cdot\mathbf{r})] \quad (9)$$

where $\Delta\mathbf{k}^{\pm} = k[\pm\sin\theta_r\hat{\mathbf{x}} - (1+\cos\theta_r)\hat{\mathbf{y}}]$ measures the intensity modulation strength. The expressions for functions $G(x)$ and $F(y)$ can be written as

$$F(y) = (R_1^2 - R_2^2)\sin\theta_r y \quad (10)$$

$$G(x) = [1 - (R_1^2 + R_2^2)\cos\theta_r]x - \frac{R_1R_2}{k}\frac{\cos\theta_r}{\sin\theta_r}\sin(2k_x x) \quad (11)$$

where $k_x = k\sin\theta_r$. The function $g(x, y)$ is plotted in Fig. 2C. Now, we can define possible profiles of local metamirrors, shown by white lines. Among all the possible surfaces, we chose the one marked with the dashed line. We can see that the amplitude of the surface modulation is larger than that in the anomalous reflective metamirror: $t = 0.3\lambda$. The impedance associated with this curve is presented in Fig. 2D.

Figure 2E shows the real part of the scattered field obtained with numerical simulations, where the metasurface is modeled as a reactive impedance boundary. The field map shows the interface pattern of plane waves. The amplitudes of the reflection coefficients in this numerical study are $|R_1| = 1.43$ and $|R_2| = 0.92$. This result is in agreement with the design criteria. For the actual implementation, we can use the same configuration where the desired impedance is fulfilled by rigidly ended tubes of different lengths. Figure 2F shows the results of a numerical simulation of a real structure that produces the desired response. The two reflected waves carry 70 and 29% of the incident power. The small discrepancy is caused by the discretization of the ideally continuous surface, as in any other metasurface designs. For improvement, we need to ensure that the impedance profile is smoothly represented by an array of discrete phase shifters.

Experimental verification

The theory is then verified by experiments. As a proof-of-concept demonstration, we choose an acoustic metamirror capable of reflecting normally incident acoustic waves into the 70° direction. The metamirror is composed of 3D-printed closed-end tubes, where the surface geometry follows the conformal contour perpendicular to the power flow direction, as illustrated in Fig. 1F. The operational frequency is chosen to be 3000 Hz, and the width of each tube is 8 mm, smaller than 0.1λ. The length of a period of the fabricated sample is 12 cm, with a thickness of 6.3 cm, around half of the operational wavelength. A photo of one segment of the fabricated sample with three periods is shown Fig. 3A. The final sample consists of 12 periods.

In the experimental verification, we use a spatially modulated Gaussian beam to illuminate the sample (see Methods for more details about the simulation and the experimental beam generation). To obtain the scattered fields, we perform two measurements. First, the sample is placed in the setup, and the total field is acquired, i.e., the sum of incident and scattered fields. The incident field and parasitic scattering from the setup are removed by subtracting the fields measured in the absence of the sample. The left panels of Fig. 3 (C and D) show the real part and magnitude of the scattered fields by the metamirror when the width of the beam is $w_0 =$ 40 cm. In these results, we can see that more energy goes into the desired direction; however, there is a residual amount of energy scattered into other directions.

This imperfection is a consequence of the finite width of the beam. It is important to notice that the sample has been designed for a plane wave–to–plane wave transformation and it is not optimized for the transformation of beams. For wider beams, the performance of the metamirror is better. For a deeper analysis of this feature, one can compare the performance of the metamirror when it is illuminated with different beams. Specifically, we compare the simulated response of the conformal metamirror when the beam width is 40 and 60 cm. We further analyze the efficiency by performing Fourier transform on the fields along the line exiting the metamirror, and the results are shown in

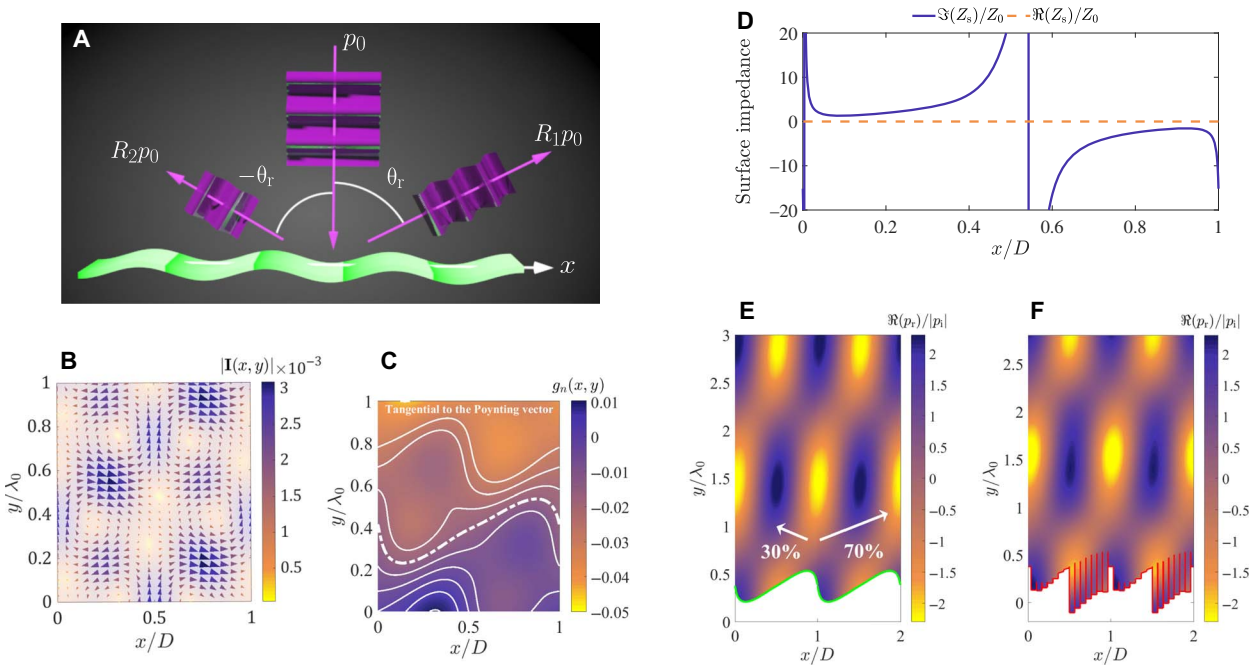

Fig. 2. Asymmetric beam splitter (70 and 30%). The analysis is carried out for $\phi_1 = \phi_2 = 0$, $\theta_i = 0°$, and $\theta_r = \pm 70°$. (**A**) Schematic representation of the problem. (**B**) Distribution of the intensity. The period of the metasurface equals $D = \lambda_0/|\sin\theta_i - \sin\theta_r|$, where λ_0 is the wavelength at the operation frequency. (**C**) The normalized curve level function $g_n(x, y) = g(x, y)/I_0$. White lines represent the level curves, i.e., the curves parallel to the intensity vector. (**D**) Surface impedance. The corresponding level curve associated with this impedance is marked with the dashed line in (C). Numerical results for the power-conformal metasurface: (**E**) Metasurface modeled as an impedance boundary. The green line shows the position of the boundary. (**F**) Actual implementation using rigidly ended tubes. Red lines show tube walls modeled as hard boundaries.

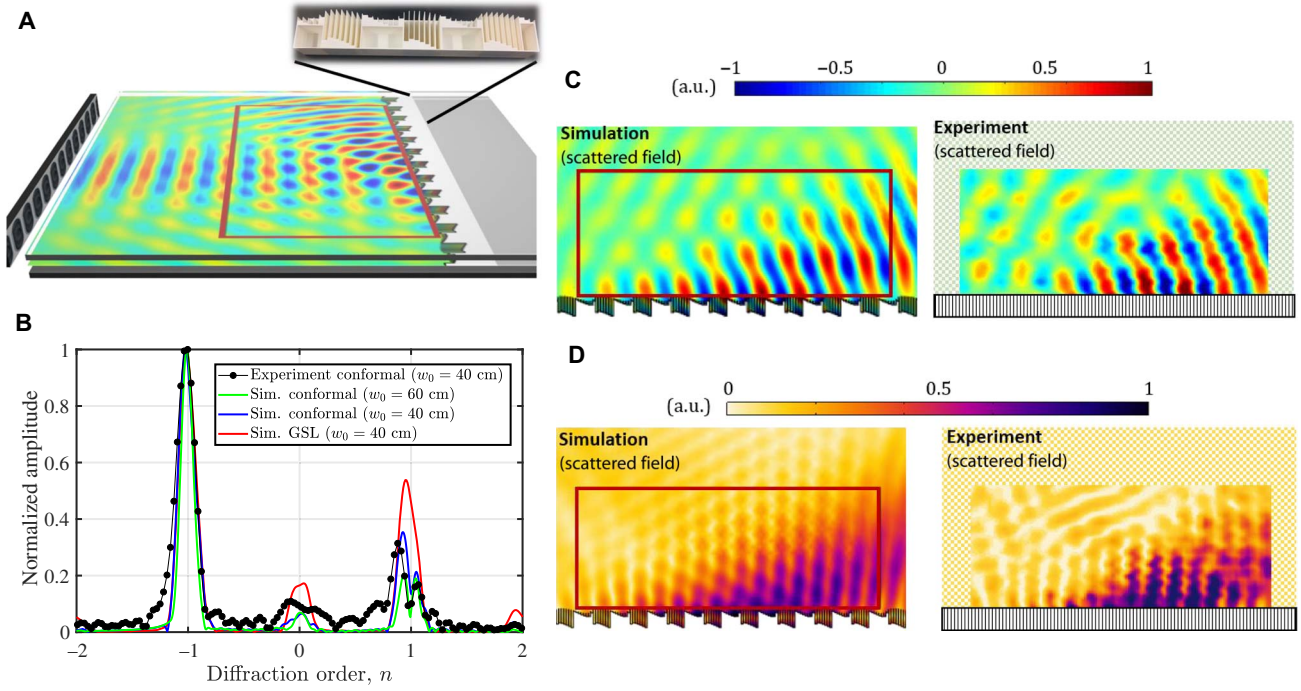

Fig. 3. Experimental verification. (**A**) Schematic representation of the experimental setup and a photograph of the fabricated sample. (**B**) Comparison between the normalized scattering of the anomalous reflective metamirrors for different beam widths, w_0: simulation (sim.) of the conformal metamirror (w_0 = 40 and 60 cm), experimental verification of the conformal metamirror (w_0 = 40 cm), and simulated GSL design (w_0 = 40 cm). The normalized scattering is calculated with a Fourier transform of the pressure fields along a line over the metasurfaces. (**C** and **D**) Analysis of the real part (C) and the magnitude square (D) of the experimental pressure field and the comparison with numerical simulations. a.u., arbitrary units.

Fig. 3B. From this analysis, we can see that the energy scattered into an undesired direction is markedly reduced when the width of the beam increases. To compare these results with our theoretical predictions, we calculate the efficiency with the energy confined only in three plane waves with $k_x = k_0\sin(70°)$, $k_x = 0$, and $k_x = -k_0\sin(70°)$ (see Methods for more details about this calculation). With this definition, the simulated efficiencies are $\eta_{40}^{\mathrm{sim}} = 97\%$ and $\eta_{60}^{\mathrm{sim}} = 98\%$. For comparison purposes, the simulated results of a GSL-based metamirror implemented with the same number of elements are also included. The efficiency of this design is $\eta_{40}^{\mathrm{GSL}} = 77\%$ (the theoretical limit for GSL-based designs with this configuration is 76%, and the small disagreement is attributed to numerical errors in the simulation and the calculation of the efficiency). We can conclude that the efficiency of the conformal metamirror is higher than that of the corresponding conventional design.

The sample is secured in a 2D waveguide for field mapping; the detailed experimental setup is described in Methods. Figure 3 (C and D) shows the simulated and measured acoustic fields at 3000 Hz. Excellent agreement can be observed, and it can be seen that the reflected field mainly contains the 70° wave component. The small discrepancies may be attributed to nonperfect Gaussian beam generation, fabrication errors, and inevitable dissipation loss. The Fourier analysis result is shown in Fig. 3B, where we can confirm the agreement with the simulations. In both simulations and experiments, almost all of the energy is confined in $k_x = k_0\sin(70°)$, which is the desired direction of the outgoing wave. The measured efficiency of the metamirror is 96.9%, which validates our approach. This efficiency is calculated from the scattered energy; i.e., the absorption produced in the narrow channels of the structure is not taken into account.

The losses of the system can be quantified using corresponding finite element method simulations. For this purpose, the linearized Navier-Stokes description is used. The results of this simulation show that viscothermal effects reduce the efficiency to 92.2%. The rest of the energy is either scattered into other directions (2.9%) or absorbed at the boundary layers (4.9%). It is important to mention that the normalization of this result to the scattered power supports our experimental findings. The effect of losses can be mitigated by reducing the number of phase shifters per period, which yields wider channels (see the Supplementary Materials).

DISCUSSION

Here, we have introduced a multiphysics design method for the creation of acoustic or electromagnetic metamirrors for general shaping of reflected waves. Examples of anomalous reflectors and beam splitters have been provided. The proposed local, passive, and lossless structures ensure theoretically perfect performance for arbitrary deflection angles, extending the range of accessible functionalities of both diffraction gratings and phase-gradient reflective metasurfaces. It is important to stress that the introduced design approach does not require any numerical optimizations, offering full physical insight into complex reflection and diffraction phenomena and giving a clear advantage in practical device design. The experimental validation reported in this work is the first implementation of an anomalous reflective acoustic metamirror that overcomes the efficiency limitations of GSL-based designs.

Conformal metasurfaces have been used to create cloaking devices, optical or acoustic illusions, and lenses. In all these examples, conformal metasurfaces are thought to adapt to the shape of scattering or reflecting bodies (*27*). Here, we have proposed a concept of conformal metasurfaces that adapt to the desired power distribution of the fields. Since this concept is applicable in all scenarios where the gradient of the desired field structure is continuous, it can be used to realize various complex field transformations with high efficiency, such as focusing or beam shaping. In addition, the use of this general method in the transmission scenario has yet to be investigated. To this end, conformal metasurfaces with double modulation (two sides of the metasurface can be engineered) and bianisotropic response could provide "boundary conditions" that warrant passivity and locality (continuity of the normal component of the intensity vector along the metasurface) (*16*, *20*, *28*, *29*).

METHODS

Numerical simulations

The simulations were performed with the commercial finite element analysis solver COMSOL Multiphysics. The infinite systems were modeled by one period using Floquet periodic conditions. The simulation shown in Figs. 1E and 2E was calculated with impedance boundaries, defining the values according to impedances shown in Figs. 1D and 2D. The simulation of the proposed designs (see Figs. 1F and 2F) was calculated using sound hard boundary conditions. In these simulations, the illumination is a perfect plane wave implemented using background pressure field domain conditions.

For the simulations of the experiment, we used a finite number of periods and Gaussian beam illumination. The Gaussian beam propagating in y direction is expressed as

$$p_{\mathrm{i}} = p_0 \frac{w_0}{w(y)} e^{\frac{-x^2}{w(y)^2}} e^{-jk\frac{x^2}{2R(y)}} e^{jk(y-y_0)} e^{-j\eta(y)} \tag{12}$$

where p_0 is the beam amplitude, w_0 is the spot radius, $w(y) = w_0\sqrt{1+\left(\frac{y-y_0}{y_{\mathrm{R}}}\right)^2}$ defines the spot size variation as a function of the distance from the beam waist, $y_{\mathrm{R}} = \pi w_0^2/\lambda$ is the Rayleigh range, $R(y) = (y-y_0)\left[1+\left(\frac{y_{\mathrm{R}}}{y-y_0}\right)^2\right]$ is the curvature radius, and $\eta(y) = \arctan\left(\frac{y-y_0}{y_{\mathrm{R}}}\right)$ is the phase change close to the beam waist. The boundaries of the metasurface were set as hard walls. The background medium was modeled as a semicircle with a radius of 1.2 m using plane wave radiation conditions. The excitation was implemented using background pressure field domain conditions. The wall of the metasurface was modeled using sound hard boundary conditions.

Field mapping measurements

The samples tested were fabricated with fused deposition modeling 3D printing where the printed material is acrylonitrile butadiene styrene plastic with a density of 1180 kg/m^3 and a speed of sound of 2700 m/s. The walls were considered to be acoustically rigid since the characteristic impedance of the material was much larger than that of air. A loudspeaker array with 28 speakers sends a Gaussian-modulated beam normally to the metasurface, and the field was scanned using a moving microphone at a step of 2 cm. The acoustic field at each spot was then calculated using Fourier transform (*30*). The reflected field was calculated by filtering out the incident using 2D Fourier transform. The overall scanned area was 100 cm by 40 cm, and the signal at each position was averaged out of four measurements to reduce noise.

Measurement of the efficiency

The efficiency of the metasurface when the metasurface is illuminated by a Gaussian beam cannot be extracted directly from the amplitude of

the reflected beam. Because of the multiple wave numbers associated with the finite size beam, this amplitude can be distorted. For an accurate calculation of the efficiency, we used the Fourier transform of the pressure fields along a line over the metasurface (see Fig. 3B).

This analysis gives the amplitude of all the Fourier components. However, to calculate the efficiency, we only used the amplitudes of the $n = -1, 0, 1$ harmonics, which corresponded to the propagating waves at 70°, 0°, and −70°. The power carried by each component was calculated as $P_n = A_n^2 \cos\theta_n$, where A_n is the amplitude of the n harmonic and θ_n defines the direction of propagation. Last, the efficiency of the metasurface can be calculated as

$$\eta = \frac{P_{-1}}{\sum_{n=-1,0,1} P_n} \tag{13}$$

It is important to notice that in this definition of the efficiency, the dissipation losses are not included.

SUPPLEMENTARY MATERIALS

Supplementary material for this article is available at http://advances.sciencemag.org/cgi/content/full/5/2/eaau7288/DC1

Section S1. Formulation for electromagnetic fields

Section S2. Discretization analysis

Fig. S1. Schematic representation of the scenarios under study.

Fig. S2. Power flow–conformal metamirror for an electromagnetic anomalous reflection when $\theta_i = 0°$ and $\theta_r = 70°$.

Fig. S3. Power flow–conformal metamirror for an electromagnetic beam splitter when $\theta_i = 0°$, $\theta_{r1} = 70°$, $\theta_{r2} = -70°$, and $\phi_{r1} = \phi_{r2} = 0$ and 70 and 30% of the energy are sent into $\pm\theta_r$.

Fig. S4. Scattered fields for different numbers of elements per period when $\theta_i = 0°$ and $\theta_r = 70°$.

Table S1. Efficiency of the conformal anomalous reflector for different numbers of elements per period when $\theta_i = 0°$ and $\theta_r = 70°$.

REFERENCES AND NOTES

1. N. Yu, F. Capasso, Flat optics with designer metasurfaces. *Nat. Mater.* **13**, 139–150 (2014).
2. S. B. Glybovski, S. A. Tretyakov, P. A. Belov, Y. S. Kivshar, C. R. Simovski, Metasurfaces: From microwaves to visible. *Phys. Rep.* **634**, 1–72 (2016).
3. C. L. Holloway, E. F. Kuester, J. A. Gordon, J. O'Hara, J. Booth, D. R. Smith, An overview of the theory and applications of metasurfaces: The two-dimensional equivalents of metamaterials. *IEEE Antennas Propag. Mag.* **54**, 10–35 (2012).
4. N. Yu, P. Genevet, M. A. Kats, F. Aieta, J.-P. Tetienne, F. Capasso, Z. Gaburro, Light propagation with phase discontinuities: Generalized laws of reflection and refraction. *Science* **334**, 333–337 (2011).
5. N. Bonod, J. Neauport, Diffraction gratings: From principles to applications in high-intensity lasers. *Adv. Opt. Photonics* **8**, 156–199 (2016).
6. E. Popov, L. Tsonev, D. Maystre, Gratings—General properties of the Littrow mounting and energy flow distribution. *J. Mod. Opt.* **37**, 367–377 (1990).
7. A. L. Kitt, J. P. Rolland, A. N. Vamivakas, Visible metasurfaces and ruled diffraction gratings: A comparison. *Opt. Mater. Express* **5**, 2895–2901 (2015).
8. Y. Ra'di, D. L. Sounas, A. Alù, Metagratings: Beyond the limits of graded metasurfaces for wave front control. *Phys. Rev. Lett.* **119**, 067404 (2017).
9. A. Epstein, O. Rabinovich, Unveiling the properties of metagratings via a detailed analytical model for synthesis and analysis. *Phys. Rev. Appl.* **8**, 054037 (2017).
10. V. S. Asadchy, Y. Ra'di, J. Vehmas, S. A. Tretyakov, Functional metamirrors using bianisotropic elements. *Phys. Rev. Lett.* **114**, 095503 (2015).
11. S. Sun, K.-Y. Yang, C.-M. Wang, T.-K. Juan, W. T. Chen, C. Y. Liao, Q. He, S. Xiao, W.-T. Kung, G.-Y. Guo, L. Zhou, D. P. Tsai, High-efficiency broadband anomalous reflection by gradient meta-surfaces. *Nano Lett.* **12**, 6223–6229 (2012).
12. Y. Li, B. Liang, Z.-m. Gu, X.-y. Zou, J.-c. Cheng, Reflected wavefront manipulation based on ultrathin planar acoustic metasurfaces. *Sci. Rep.* **3**, 2546 (2013).
13. J. Zhao, B. Li, Z. Chen, C.-W. Qiu, Manipulating acoustic wavefront by inhomogeneous impedance and steerable extraordinary reflection. *Sci. Rep.* **3**, 2537 (2013).
14. K. Song, J. Kim, S. Hur, J.-H. Kwak, S.-H. Lee, T. Kim, Directional reflective surface formed via gradient-impeding acoustic meta-surfaces. *Sci. Rep.* **6**, 32300 (2016).
15. W. Wang, Y. Xie, B.-I. Popa, S. A. Cummer, Subwavelength diffractive acoustics and wavefront manipulation with a reflective acoustic metasurface. *J. Appl. Phys.* **120**, 195103 (2016).
16. V. S. Asadchy, M. Albooyeh, S. N. Tcvetkova, A. Díaz-Rubio, Y. Ra'di, S. A. Tretyakov, Perfect control of reflection and refraction using spatially dispersive metasurfaces. *Phys. Rev. B* **94**, 075142 (2016).
17. N. M. Estakhri, A. Alù, Wave-front transformation with gradient metasurfaces. *Phys. Rev. X* **6**, 041008 (2016).
18. A. Díaz-Rubio, V. S. Asadchy, A. Elsakka, S. A. Tretyakov, From the generalized reflection law to the realization of perfect anomalous reflectors. *Sci. Adv.* **3**, e1602714 (2017).
19. A. Epstein, G. V. Eleftheriades, Synthesis of passive lossless metasurfaces using auxiliary fields for reflectionless beam splitting and perfect reflection. *Phys. Rev. Lett.* **117**, 256103 (2016).
20. A. Díaz-Rubio, S. A. Tretyakov, Acoustic metasurfaces for scattering-free anomalous reflection and refraction. *Phys. Rev. B* **96**, 125409 (2017).
21. V. S. Asadchy, A. Wickberg, A. Díaz-Rubio, M. We-gener, Eliminating scattering loss in anomalously reflecting optical metasurfaces. *ACS Photonics* **4**, 1264–1270 (2017).
22. D.-H. Kwon, S. A. Tretyakov, Perfect reflection control for impenetrable surfaces using surface waves of orthogonal polarization. *Phys. Rev. B* **96**, 085438 (2017).
23. D.-H. Kwon, Lossless scalar metasurfaces for anomalous reflection based on efficient surface field optimization. *IEEE Antennas Wirel. Propag. Lett.* **17**, 1149–1152 (2018).
24. V. S. Asadchy, A. Díaz-Rubio, S. N. Tcvetkova, D.-H. Kwon, A. Elsakka, M. Albooyeh, S. A. Tretyakov, Flat engineered multichannel reflectors. *Phys. Rev. X* **7**, 031046 (2017).
25. COMSOL AB, COMSOL Multiphysics, v. 5.3.; www.comsol.com.
26. F. Jacobsen, P. M. Juhl, *Fundamentals of General Linear Acoustics* (John Wiley & Sons, 2013).
27. J. Y. H. Teo, L. J. Wong, C. Molardi, P. Genevet, Controlling electromagnetic fields at boundaries of arbitrary geometries. *Phys. Rev. A* **94**, 023820 (2016).
28. J. Li, C. Shen, A. Díaz-Rubio, S. A. Tretyakov, S. A. Cummer, Systematic design and experimental demonstration of bianisotropic metasurfaces for scattering-free manipulation of acoustic wavefronts. *Nat. Commun.* **9**, 1342 (2018).
29. J. Li, A. Díaz-Rubio, C. Shen, Z. Jia, S. Tretyakov, S. Cummer, Perfect generation of angular momentum with cylindrical bianisotropic metasurfaces. arXiv:1806.04349 (2018).
30. B.-I. Popa, L. Zigoneanu, S. A. Cummer, Experimental acoustic ground cloak in air. *Phys. Rev. Lett.* **106**, 253901 (2011).

Acknowledgments

Funding: This work was supported by the Academy of Finland (projects 287894 and 309421) and by a Multidisciplinary University Research Initiative grant from the Office of Naval Research (N00014-13-1-0631). **Author contributions:** A.D.-R. developed the mathematical model and designed samples. A.D.-R., J.L., and C.S. performed numerical simulations. J.L. and C.S. fabricated samples and performed experiments. S.A.C. and S.A.T. supervised the project. All authors discussed the results and prepared the manuscript. **Competing interests:** The authors declare that they have no competing interests. **Data and materials availability:** All data needed to evaluate the conclusions in the paper are present in the paper and/or the Supplementary Materials. Additional data related to this paper may be requested from the authors.

Submitted 10 July 2018
Accepted 4 January 2019
Published 15 February 2019
10.1126/sciadv.aau7288

Citation: A. Díaz-Rubio, J. Li, C. Shen, S. A. Cummer, S. A. Tretyakov, Power flow–conformal metamirrors for engineering wave reflections. *Sci. Adv.* **5**, eaau7288 (2019).

ScienceAdvances

Power flow–conformal metamirrors for engineering wave reflections

Ana Díaz-Rubio, Junfei Li, Chen Shen, Steven A. Cummer and Sergei A. Tretyakov

Sci Adv **5** (2), eaau7288.
DOI: 10.1126/sciadv.aau7288